IEEE Access
Multidisciplinary : Rapid Review : Open Access Journal

Received April 3, 2020, accepted April 19, 2020, date of publication May 7, 2020, date of current version May 21, 2020.

Digital Object Identifier 10.1109/ACCESS.2020.2993020

Prevention and Survivability for Power Distribution Resilience: A Multi-Criteria Renewables Expansion Model

HONGGANG WANG[1] AND TONGDAN JIN[2], (Senior Member, IEEE)
[1]College of Business Administration, California State Polytechnic University-Pomona, Pomona, CA 91763, USA
[2]Ingram School of Engineering, Texas State University, San Marcos, TX 78666, USA

Corresponding author: Tongdan Jin (tj17@txstate.edu)

This work was supported in part by the U.S. NSF CBET Program under Grant 1704933.

ABSTRACT Distributed energy resources are capable of enhancing grid resilience through island operations in contingency. This paper proposes a multi-year, multi-criteria generation expansion model to achieve distribution power resilience through renewable energy integration. In cases that distribution circuits or fuel lifeline are destroyed post natural disasters, wind- and solar-based generators form island microgrids to power the critical load. The goal is to determine the sizing, siting and maintenance of distributed energy resources such that system cost and power shortage in contingency are minimized. Moment methods and central limit theorem are used to characterize the spatial climate uncertainty, generation intermittency, and voltage variation. The research contributions are twofold. First, the expansion model achieves triple goals by meeting the annual load growth, reducing the carbon footprint, and enhancing the grid resilience manifested as prevention and survivability. Second, we present an improved direct zigzag algorithm to search for the Pareto solutions. Numerical examples show that the zigzag search outperforms evolutionary-based algorithms as it can identify higher-quality non-dominant solutions by exploring a wider Pareto frontier.

INDEX TERMS Power resilience, island microgrid, prevention and survivability, zigzag algorithm, chance constraint.

I. INTRODUCTION

At present physical hardening and distributed generation (DG) are the two primary approaches to enhancing the resilience of distribution grid. Adding redundant overhead lines and backup generation, fortifying poles, trimming vegetation, and preventive maintenance all fall into the hardening category [1]–[3]. The second approach for resilience attainment is to design and implement active distribution grid in which microgrid systems or distributed energy resources (DER), such as wind turbine, photovoltaic system, and battery energy storage, can operate in island mode to power the critical load post the disaster attacks [4], [5]. The global installation of DER units and microgrid capacity consistently increases, making the distribution grid more active in power supply. The study [6] shows that in 2012 alone, the world-wide new installation of DER reached 142 GW, representing 39% share of the new capacity addition of that year. The rise of active distribution systems opens the way of deploying resilient smart grid via microgrid generation [7], [8].

EPRI [9] interprets and defines the grid resiliency in three aspects: 1) prevention, 2) survivability, and 3) recovery. Prevention aims to avoid or mitigate the distribution system damage. Survivability includes the use of backup, mobile or distributed generating units to maintain some basic electricity supply to critical loads. Recovery ought to provide for rapid damage assessment, prompt crew deployment to damaged sites and readily available replacement components.

This paper aims to design a resilient distribution system against disastrous weather events through the progressive integration of wind- and solar-based DER units. We propose a multi-criteria distributed generation expansion model to achieve prevention and survivability performance. In our model, prevention is achieved by allocating DER units and adopting preventive maintenance. Survivability is attained through the island microgrid operation in contingency. In case that several or all distribution lines are damaged or

The associate editor coordinating the review of this manuscript and approving it for publication was Kai Li.

This work is licensed under a Creative Commons Attribution 4.0 License. For more information, see https://creativecommons.org/licenses/by/4.0/

disconnected, renewable DER units can be clustered and form island microgrid systems to power the critical loads.

The remainder of the paper is organized as follows. Section II reviews the probabilistic DG planning models. Sections III performs the cost analysis of the DG system. Section IV characterizes the voltage variation and bidirectional power flow. In Section V a multi-criteria DG expansion model featured with prevention and survivability is formulated under generation uncertainty. In Section VI, we demonstrate the computational efficiency of the zigzag optimization algorithm in a 13-node distribution network. Section VII concludes the paper.

NOMENCLATURE

Notation	Description
$i =$	index for the type of DER unit.
$j =$	index for the node of the distribution network.
$t =$	index for the planning year.
$l =$	index for the power line between two adjacent nodes.
$m =$	number of DER types, for $i = 1, 2, \ldots, m$.
$n =$	number of nodes for placing DER, for $j = 1, 2, \ldots, n$.
$T =$	number of planning years, for $t = 1, 2, \ldots, T$.
$J =$	number of nodes along a feeder for $j = 1, 2, \ldots, J$.
$P_{ijt} =$	power output of DER type i at node j in year t, a random variable.
$D_i =$	load of node i, random variable.
$L_l =$	load of line l, and $l = 1, 2, \ldots, n$-1, random variable.
$P_i^c =$	power capacity of DER type i.
$r =$	annual discount factor.
$a_{ij} =$	DER capacity cost (\$/MW) for type i at node j.
$b_{ij} =$	DER operating cost (\$/MWh) for type i at node j.
$c_{ij} =$	carbon credits (\$/MWh) for DER type i at node j.
$d_{ij} =$	subsidies (\$/MW) of DER type i at node j.
$t_i^a =$	annual operating time for DER type i.
$F_i(y) =$	cumulative distribution function for lifetime of DER type i.
$f_i(y) =$	probability density function for lifetime of DER type i.
$R_i(y) =$	reliability function of DER type i.
$\eta_i, \beta_i =$	scale and shape parameters of Weibull reliability function.
$t_i^f, t_i^p =$	downtime duration for DER type i in a corrective and a scheduled maintenance, respectively.
$u_i(\tau_i) =$	maintenance cost rate for DER type i.
$R_l =$	resistance of link l, for $l = 1, 2, \ldots, n-1$.
$I_l =$	current in link l, for $l = 1, 2, \ldots, n-1$, random variable.
$V_j =$	voltage of node j, for $j = 1, 2, \ldots, n$, random variable.
$V_{DG} =$	nominal voltage of the distribution network.
$c_w, d_w =$	scale and shape parameters of Weibull wind speed distribution.
$s_m =$	maximum solar irradiance on PV in a year.
$a_s, b_s =$	shape parameters of the beta distribution.
$\lambda_t =$	green energy coefficient in year t, for $t = 1, 2, \ldots, T$.
$x_{ijt} =$	installation of DER type i at node j in year t, binary decision variable.
$\tau_i =$	maintenance interval for DER type i, decision variable.
$\omega =$	random wind profile or solar irradiance.
$\xi =$	random consumption activity of nodal power.

II. LITERATURE REVIEW

A large body of literature pertaining to DG siting and sizing is available, and readers are referred to the recent survey by Georgilakis and Hatziargyriou [10]. The main objective of DG planning is to allocate DER units in distribution networks to optimize the system performance, such as cost, reliability, power quality and carbon emissions. In these studies, grid resilience features such as prevention and survivability are not explicitly incorporated in the DER siting and sizing model.

Recently, grid resilience is emerging as a key criterion to measure how a power system can survive and withstand under extreme weather or unusual events. Panteli *et al.* [11] use a set of severity risk index to determine the application of defensive islanding of power grid in extreme weather. It boosts the grid resilience by splitting the network into stable and self-adequate islands in order to isolate the components with higher failure probability, especially cascading failures. Kwasinski *et al.* [12] compare the availability of different DER units upon natural disaster onslaught. Their study shows that wind turbine (WT) and solar photovoltaic (PV) outperform fuel-based generators because the lifeline of fuel supply is likely damaged after the harsh weather or earthquake. Bie *et al.* [13] propose a quantitative framework along with several metrics (i.e. LOLP and EDNS) to evaluate power grid resilience, extending the scope of reliability measures to resilience measures. Ma *et al.* [14] propose a resilience-oriented design framework via line hardening, backup DG, and use of automatic switches. A two-stage mixed-integer stochastic optimization incorporating spatio-temporal correlation uncertainties is formulated to minimize the cost of investment, loss of load, DG operation, and damage repairs. Liu *et al.* [15] use Monte Carlo simulation to compare the grid resilience between network hardening, topology reconfiguration and microgrid operations based on IEEE 30-bus and 118-bus systems. Their study shows that topology reconfiguration and microgrid operations could outperform network hardening under extreme events.

To continuously supply electric power under extreme weather conditions, we propose a distributed generation expansion model by minimizing the maximum nodal power shortage when all or certain distribution lines are disconnected post disaster attack. The contributions of this paper are highlighted in following:

- The proposed DG expansion model achieves triple goals: meeting the annual load growth, reducing carbon footprint, and enhancing grid resilience manifested as prevention and survivability. The novelty of our work is to incorporate prevention and survivability features into the traditional DG expansion process.
- Island microgrid operation is designed into the distribution system through onsite wind and solar generation. Hence, it can avoid cascading failures resulted from common cause failures, such as damaged fuel supply infrastructure.
- We present an improved direct zigzag search algorithm to solve the multi-criteria optimization model by exploring a wider Pareto front.

III. SYSTEM RESILIENCE AND COST ANALYSIS

A. THREE LEVELS OF RESILIENCE

Figure 1 depicts five resilience states that evolve with time upon the extreme event attack: reliability, degradation, stabilization, recovery or repair, and renewed state. Let $P(t)$ be the power at time t, three different levels of grid resilient behavior are explained below.

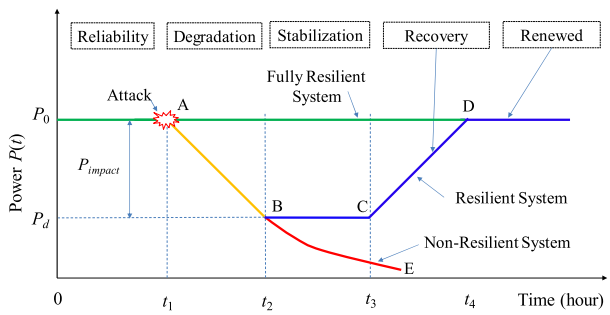

FIGURE 1. Resilient system vs. non-resilient system.

Level 1: If WT, PV and battery are adopted as DER in the distribution grid, the grid is able to meet the load with no significant performance degradation provided the battery capacity is large enough. Such design is referred to as 'fully' resilient system as shown by path AD.

Level 2: If only WT and PV are adopted, $P(t)$ is likely to decline due to their intermittent generation and the potential loss of substation. Path AB represents the degradation process. The design objective is to ensure that the average power from WT and PV remains at P_d. In that way, the critical loads within a node still can be energized from time t_2, At t_3 the system starts to recover and eventually return to P_0 at t_4. Since critical loads are energized in $[t_1, t_4]$, the grid operating with path ABCD is also treated as a resilient system.

Level 3: If there is no WT and PV or other DER units, $P(t)$ will continue to drop after t_2. The grid power eventually crashes at t_3 if all the lines are disconnected or the substation is damaged. Therefore, the system is considered as a non-resilient design.

Our model is presented at Level 2 where the distribution grid may lose certain amounts of power post the extreme event. Since WT and PV units could accelerate the power restoration by reducing the recovery time, this is another value-added resilience feature of onsite generation. The restoration becomes more difficult and takes a longer time if the grid is completely down.

B. SYSTEM COST ANALYSIS

The cost of a DG system comprises of four main items: installation, operating and maintenance, carbon credits, and equipment subsidies. Let i be the index of available DER types for $i = 1, 2, \ldots, m$. Further let $x_{ijt} \in \{0, 1\}$ be the binary decision variable representing DER type i is installed at node j for $j = 1, 2, \ldots, n$ in year t for $t = 1, 2, \ldots, T$. The present worth of DG cost over a period of T years, C_{eq}, can be estimated by

$$C_{eq} = \sum_{t=1}^{T} \left((1+r)^{1-t} \sum_{i=1}^{m} \sum_{j=1}^{n} x_{ijt} a_{ij} P_i^c \right), \tag{1}$$

where a_{ij} is the capacity cost (\$/MW) of DER type i at node j, and P_i^c is the power capacity for DER type i. Parameter r is the discount factor. Though wind and solar generation does not require fuels, the costs of leasing the land for equipment placement is treated as part of the capacity cost.

WT and PV are prone to field failures. System reliability and availability can be improved through preventative maintenance (PM) by pro-actively inspecting and replacing aging components. Age-based PM is perhaps the most widely used maintenance policy in power industry because of the scheduling flexibility [16], [17]. The cost rate in [17] is adopted to estimate the maintenance expense. Let C_{mn} be the maintenance cost of the DG system over T years, then

$$\begin{aligned} C_{mn} &= \sum_{t=1}^{T} (1+r)^{1-t} \sum_{i=1}^{m} \sum_{j=1}^{n} t_i^a z_{ijt} u_i(\tau_i) \\ &= \sum_{t=1}^{T} (1+r)^{1-t} \sum_{i=1}^{m} \sum_{j=1}^{n} t_i^a z_{ijt} \\ &\quad \times \left(\frac{c_i^f F_i(\tau_i) + c_i^p R_i(\tau_i)}{\tau_i R_i(\tau_i) + F_i(\tau_i) \int_0^{\tau_i} f_i(y) y dy} \right) \end{aligned} \tag{2}$$

With

$$f_i(y) = \left(\frac{\beta_i}{\eta_i}\right) \left(\frac{y}{\eta_i}\right)^{\beta_i - 1} e^{-\left(\frac{y}{\eta_i}\right)^{\beta_i}}. \tag{3}$$

where τ_i is the decision variable representing the PM interval, and $u_i(\tau_i)$ is the maintenance cost rate of DER type i during a PM cycle. Here t_i^a is the annual operating hours of DER type i, and $z_{ijt} = \sum_{k=1}^{t} x_{ijk}$ is the cumulative DER units of type i installed at node j through year t. Note that $F_i(y)$ and $f_i(y)$ are, respectively, the Weibull cumulative distribution function and the probability density function, and η_i and β_i are the scale and shape parameters, respectively. $R_i(\tau_i)$ is the reliability of DER type i, and $R_i(\tau_i) = 1\text{-}F_i(\tau_i)$. Weibull distribution is widely used to model the failure probability of WT and PV

units [18], [19]. Finally, c_i^f is the cost of a corrective maintenance action, and c_i^p is the cost of a scheduled maintenance action on generation type i.

The operating cost of the distribution grid is the expenses associated with the routine equipment checking, line inspection and trimming of vegetation. Based on [20], The operating cost, denoted as C_{op}, is assumed to be proportional to the energy generated

$$C_{op} = \sum_{t=1}^{T} \left((1+r)^{1-t} \sum_{i=1}^{m} \sum_{j=1}^{n} t_i^a z_{ijt} b_{ij} P_{ijt} \right), \tag{4}$$

where b_{ij} is the operating cost per MWh of electricity generated from DER type i at node j. The justification of Equation (4) is that tear and wear on turbines, solar PV, and distribution circuits likely increase with energy generation [20]. Some studies treat annual operating and maintenance cost as a fixed quantity, but others prefer to use cost per MWh (e.g. \$/MWh). In this paper C_{op} is assumed to be proportional to the energy delivered.

Carbon credits and equipment subsidies aim to incentivize the adoption of WT or PV units. Let c_{ij} be the credits given to the DER type i at node j whenever one MWh of renewable energy is produced. Also let d_{ij} be the subsidies per MW capacity of DER type i at node j. The present worth of total incentives received by the DG system over T years, denoted as C_{in}, can be estimated as

$$C_{in} = \sum_{t=1}^{T} \left((1+r)^{1-t} \sum_{i=1}^{m} \sum_{j=1}^{n} t_i^a z_{ijt} c_{ij} P_{ijt} \right) + \sum_{t=1}^{T} \left((1+r)^{1-t} \sum_{i=1}^{m} \sum_{j=1}^{n} x_{ijt} d_{ij} P_i^c \right). \tag{5}$$

The incentives can be treated as the cost savings for renewable DG system, hence $c_{ij} < 0$ and $d_{ij} < 0$ in equation (5).

IV. VOLTAGE VARIATION ANALYSIS

A. BIDIRECTIONAL POWER FLOW

Though quite a few direct current (DC) transmission lines are now in place worldwide, the majority of distribution grids still operate in alternating current (AC) mode. To maintain the voltage stability, capacitor banks are required and used as the Volt/Var compensators in AC grid. Since electric vehicles, battery storage, and solar PV use or generate DC power, recently the design of DC distribution systems is receiving much attention in academia and industry. A major advantage of using DC grid is its simplicity in computation and control. Comparative studies have been performed to justify and validate the use of DC power flow model [21], [22], and their conclusion is that DC power flow model is reasonably accurate to represent AC power flow systems in strategic planning, such as long-term generation expansion.

We adopt the DC power flow model from [23] to demonstrate the multi-criteria DG expansion model on the basis that the planning is performed at the strategic level for multiple

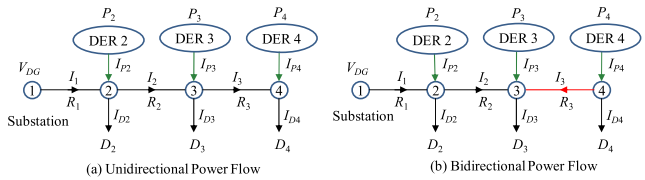

FIGURE 2. Direction of power flow under DER integration [23].

years. By referring to a single distribution line in Figure 2(a), the DC current in link j is

$$I_j \cong \frac{1}{V_{DG}} \sum_{k=j+1}^{J} (D_k - P_k), \quad \text{for } j = 1, 2, \ldots, J-1. \tag{6}$$

where V_{DG} is the nominal voltage of the DG system, P_k and D_k are the DER power and the load of node k, and J is the total number of nodes along the line. For instance, $J = 4$ in Figure 2. For a single distribution line, the index j for link is identical to the upstream node index. Similarly, the nodal voltage is given as

$$V_j \cong V_{DG} - \frac{1}{V_{DG}} \sum_{k=2}^{J} r_k (D_k - P_k), \quad \text{for } j = 2, 3, \ldots, J. \tag{7}$$

with

$$r_k = \begin{cases} \sum_{l=1}^{k-1} R_l & \text{for } 2 \le k \le j-1, \\ \sum_{l=1}^{j-1} R_l & \text{for } j \le k \le J. \end{cases} \tag{8}$$

Note R_l is the link resistance between nodes k and $k+1$. Both equations (6) and (7) allow for estimating the line current and nodal voltage based on D_k and P_k.

For a DG system, the unidirectional power flow condition always holds as long as the DER power is absorbed by the local node. The power flows reversely only if the sum of DER power exceeds the total demands of the downstream nodes. Both equations (6) and (7) are applicable to unidirectional and bi-directional power flow.

B. VARIATION OF VOLTAGE AND CURRENT

Note that I_j and V_j in equations (6) and (7) are random variables due to the uncertainty of P_j and D_j. Since the distribution function of I_j and V_j are difficult to derive, we propose a moment approach to characterizing their stochastic behavior. Let $E[I_j]$ and $Var(I_j)$ be the mean and variance of the current of link j connecting nodes j and $j+1$. We have

$$E[I_j] \cong \frac{1}{V_{DG}} \sum_{k=j+1}^{J} (\mu_{D_k} - \mu_{P_k}), \quad \text{for } j = 1, 2, \ldots, J-1. \tag{9}$$

$$Var(I_j) \cong \frac{1}{V_{DG}^2} \sum_{k=j+1}^{J} (\sigma_{D_k}^2 + \sigma_{P_k}^2), \quad \text{for } j = 1, 2, \ldots, J-1. \tag{10}$$

where, μ_{D_k} and $\sigma^2_{D_k}$ are the mean and variance of D_k of node k. Similarly, μ_{P_k} and $\sigma^2_{P_k}$ are the mean and variance of P_k of node k. The mean and variance of the voltage at node j, denoted as $E[V_j]$ and $Var(V_j)$, can be obtained as

$$E[V_j] \cong V_{DG} - \frac{1}{V_{DG}} \sum_{k=2}^{J} r_k(\mu_{D_k} - \mu_{P_k}), \quad \text{for } j = 2, 3, \ldots, J. \tag{11}$$

$$Var(V_j) \cong \frac{1}{V_{DG}^2} \sum_{k=2}^{J} r_k^2 \left(\sigma^2_{D_k} + \sigma^2_{P_k}\right), \quad \text{for } j = 2, 3, \ldots, J. \tag{12}$$

In next section, we show that equations (9)-(12) are the foundations in controlling the thermal stress and voltage variations under generation and load uncertainty.

V. MULTI-CRITERIA DG EXPANSION MODEL

A. STOCHASTIC EXPANSION MODEL

In this section we formulate a multi-year, multi-criteria DG expansion model based on the voltage and current analysis in equations (9)-(12). The model captures spatial and temporal variations, including nodal voltage, power intermittency, load growth, and environmental concern. Subject to supply reliability, power quality, thermal stress, and emission constraints, the stochastic multi-objective optimization problem (MOOP) jointly minimizes the system cost and maximize the power resilience. Let $\mathbf{x}$ represents the DER sizing and siting of the nodes; and $\boldsymbol{\tau}$ stands for the maintenance time of DER units. The MOOP, denoted as Model P1, is formulated as follows

Model P1:

$$\begin{aligned}\text{Min: } & g_1(\mathbf{x}, \boldsymbol{\tau}) \\ &= E_\omega \sum_{t=1}^{T} (1+r)^{1-t} \left[\sum_{i=1}^{m} \sum_{j=1}^{n} (a_{ij} + d_{ij}) x_{ijt} P_i^c \right. \\ &\quad \left. + \sum_{i=1}^{m} \sum_{j=1}^{n} (b_{ij} + c_{ij}) z_{ijt} t_i^a P_{ijt}(\omega) + \sum_{i=1}^{m} \sum_{j=1}^{n} z_{ijt} t_i^a u_i(\tau_i) \right]\end{aligned} \tag{13}$$

$$\begin{aligned}\text{Min: } & g_2(\mathbf{x}, \boldsymbol{\tau}) \\ &= E_{\omega,\xi} \max_j \left\{ \max \left[\sum_{t=1}^{T} D_{jt}(\xi) - \sum_{t=1}^{T} \sum_{i=1}^{t} z_{ijt} P_{ijt}(\omega),\ 0 \right] \right\}\end{aligned} \tag{14}$$

$$\text{Subject to: } \Pr\{P_t(\mathbf{x}) < D_t\} \le \alpha_1, \quad \forall t. \tag{15}$$

$$\Pr\{V_{\min} \le V_{jt}(\mathbf{x}) \le V_{\max}\} \ge \alpha_2, \quad \forall j, \text{ and } \forall t. \tag{16}$$

$$\Pr\{I_{lt}(\mathbf{x}) \le I_l^{\max}\} \ge \alpha_3, \quad \forall l, \text{ and } \forall t. \tag{17}$$

$$\Pr\left\{ \sum_{i=1}^{m} \sum_{j=1}^{n} z_{ijt} P_{ij}(\omega) \ge \lambda_t \sum_{j=1}^{n} D_{jt}(\xi) \right\} \ge \alpha_4, \quad \forall t. \tag{18}$$

$$0 \le \lambda_1 \le \lambda_2 \le \ldots \le \lambda_T \le 1, \quad \forall t. \tag{19}$$

$$z_{ijt} = \sum_{k=1}^{t} x_{ijk}, \quad \forall i, \ \forall j \text{ and } \forall t. \tag{20}$$

$$x_{ijt} \in \{0, 1\}, \tau_i \ge 0, \quad \forall i, \ \forall j \text{ and } \forall t. \tag{21}$$

In Model P1 the objective functions and the constraints involve intermittent power $P_{ijt}(\omega)$ and uncertain load $D_{jt}(\xi)$, where ω represents random wind and solar irradiance, and ξ is the demand uncertainty. Objective function (13) minimizes the expected present worth of the DG system. Objective function (14) maximizes the resilience of the grid by minimizing the maximum nodal power shortage if adjacent links are destroyed in extreme event. This ensures that the grid has the ability to withstand extraordinary and high-impact low-probability events. A typical example is the N-90 failure in Hurricane Sandy as opposed to the classical N-1 reliability design criterion [24].

There are seven constraints in Model P1. Constraints (15) is the reliability criterion defined as the loss-of-load probability (LOLP). Constraint (16) defines the scope of the voltage variation, where $V_{\max}$ and $V_{\min}$ are the upper and lower voltage limit, respectively. Constraint (17) states the thermal stress, i.e. the current in link k, should not exceed the maximum threshold $I_l^{\max}$. Constraints (18) and (19) jointly define the green energy coefficient (GEC) target λ_t to be achieved in year t. GEC measures the percentage of energy generated by WT and PV. The values of α_i for $i = 1, 2, 3$, and 4 are within [0, 1]. Note that z_{ijt} in constraint (20) is the cumulative installation of DER type i at node j from year 1 to t. Constraints (21) simply states that τ_i is nonnegative, and up to one DER unit of type i can be placed at node j in year k. This constraint, however, can be relaxed if more than one DER unit can be installed at the same node each year.

The resilience in Model P1 is manifested as prevention and survivability. To protect the grid operation against extreme weather, we rely on DER integration and preventive maintenance strategy. This is reflected by constrain (18) where the green energy coefficient λ_t increases with DER installation. The survivability is explicitly incorporated in objective function (14) by minimizing the maximum nodal power shortage in contingency.

B. DETERMINISTIC COUNTERPART

It would be difficult, if not impossible, to directly search for the optimal $\mathbf{x}$ and $\boldsymbol{\tau}$ given the random behavior of $P_{ijt}(\omega)$ and $D_{jt}(\xi)$. To make P1 more tractable, we convert it into a deterministic counterpart as follows.

Model P2:

$$\begin{aligned}\text{Min: } & g_1(\mathbf{x}, \boldsymbol{\tau}) \\ &= E_\omega \sum_{t=1}^{T} (1+r)^{1-t} \left[\sum_{i=1}^{m} \sum_{j=1}^{n} (a_{ij} + d_{ij}) x_{ijt} P_i^c \right. \\ &\quad \left. + \sum_{i=1}^{m} \sum_{j=1}^{n} (b_{ij} + c_{ij}) z_{ijt} t_i^a P_{ijt}(\omega) + \sum_{i=1}^{m} \sum_{j=1}^{n} z_{ijt} t_i^a u_i(\tau_i) \right]\end{aligned} \tag{22}$$

$$\text{Min: } g_2(\mathbf{x}, \boldsymbol{\tau}) = E_{\omega,\xi} \max_j \left\{ \max \left[\sum_{t=1}^{T} D_{jt}(\xi) - \sum_{t=1}^{T} \sum_{i=1}^{t} z_{ijt} P_{ijt}(\omega),\ 0 \right] \right\} \tag{23}$$

$$\text{Subject to: } \mu_{P_t(\mathbf{x})} \geq \mu_{D_t} + Z_{1-\alpha_1}(\sigma^2_{P_t(\mathbf{x})} + \sigma^2_{D_t})^{1/2}, \quad \forall t \tag{24}$$

$$V_{\min} - Z_{(1-\alpha_2)/2}\sigma_{V_{jt}(\mathbf{x})} \leq \mu_{V_{jt}(\mathbf{x})} \leq V_{\max} + Z_{(1-\alpha_2)/2}\sigma_{V_{jt}(\mathbf{x})}, \quad \forall j \text{ and } \forall t. \tag{25}$$

$$\mu_{I_{lt}(\mathbf{x})} \leq I_l^{\max} - Z_{\alpha_3}\sigma_{I_{lt}(\mathbf{x})}, \quad \forall l \text{ and } \forall t \tag{26}$$

$$\mu_{P_t(\mathbf{x})} \geq \lambda_t \mu_{D_t} + Z_{\alpha_4}(\sigma^2_{P_t(\mathbf{x})} + \lambda_t^2 \sigma^2_{D_t})^{1/2}, \quad \forall t \tag{27}$$

$$0 \leq \lambda_1 \leq \lambda_2 \leq \cdots \leq \lambda_T \leq 1 \tag{28}$$

$$z_{ijt} = \sum_{k=1}^{t} x_{ijk}, \quad \forall i,\ \forall j \text{ and } \forall t \tag{29}$$

$$x_{ijt} \in \{0, 1\};\ \tau_i \geq 0. \quad \forall i,\ \forall j, \text{ and } \forall t \tag{30}$$

Both P2 and P1 have the same objective functions, but constraints (24)-(27) are now in deterministic forms converted from corresponding chance constraints (15)-(18). The detailed conversion is provided in Appendix. The transformations are made based on the normality assumption on system cost, voltage variation, and thermal stresses that are commonly used in existing works [25], [26]. Note that Z-score in constraint (24) represents the Z-value of the standard normal distribution. For instance, in constraint (24) $Z_{0.95} = 1.64$ given $\alpha_1 = 0.05$. Similar interpretations can be applied to other constraints. In our case, $P_t(\mathbf{x})$ is the aggregate DER power of n nodes. According to the central limit theorem, if nodal power and load have limited mean and variance, $P_t(\mathbf{x})$ and D_t tend to be normally distributed if n is large enough.

C. SOLUTION ALGORITHM

We modified a newly developed multi-objective optimization algorithm, called direct zigzag (DZZ) algorithm [27], and use it to find the Pareto solution for P2. The results are compared with a popular GA-based MOOP method, i.e. Non-dominated Sorting Genetic Algorithm or NSGA-II [28].

The key idea of the DZZ method is to search around the Pareto front efficiently by employing local neighborhood search procedures. The efficiency of a zigzag search is due to the expectation that an existing solution path will effectively pass through the Pareto front. But how to identify such a tight solution path close to the Pareto front is crucial for the performance of DZZ. Figure 3(a) illustrates that a DZZ search is performed on a deterministic MOOP minimization problem (i.e. DMOO) with two objective functions f_1 and f_2. DZZ first employs a direct search (derivative-free optimization based on Hooke Jeeves and neighborhood search) to find the first Pareto optimum x_1 with the minimal f_1. DZZ then iteratively performs zig and zag search to find a sequence of Pareto solutions $x_1, x_2, \ldots, x_9$.

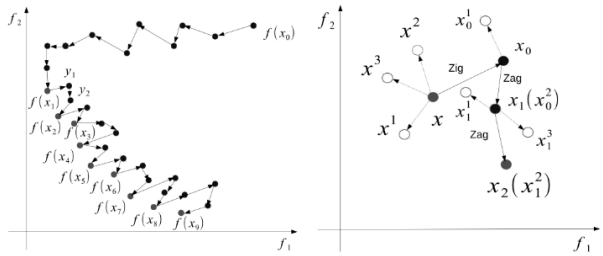

(a) DZZ for a DMOO problem. (b) Zig and zag search.

FIGURE 3. DZZ for Bi-objective optimization on f_1 and f_2.

As shown in Figure 3(b), for a bi-objective optimization with two discrete variables, a zig search is simply a neighborhood search around the current Pareto solution, say x, and returns a new and feasible solution x_0. A zag step subsequently searches neighboring points by finding x_0^1 and x_0^2 around the current candidate point for non-dominated solutions with smaller f_2 values. As shown in Figure 3(a), a zag search stops when no smaller f_2 can be found in the neighborhood of the current candidate solution.

Since Model P2 belongs to the mixed integer programing problem, we tailored DZZ to account for mixed type of decision variables $\mathbf{x}$ and τ. Note that the decision variables of installing DER units at nodes are binary, the pattern search in the Hooke Jeeves direct search is not applicable; nevertheless, pattern search for the continuous variables τ is still efficient. Thus, we apply pattern searches after every Hooke Jeeves exploration step for continuous variables.

Another enhancement of DZZ in this work is to use a broader local neighborhood search for Hooke Jeeves exploration step. The traditional Hooke Jeeves exploration searches the solutions in the smaller neighborhood $N_1(x) = \{x' : |x - x'|V \leq 1\}$ around the current candidate solution x. To find the solutions along the "valley" that is not necessarily aligned with coordinates, we consider evaluating a larger neighborhood $N_2(x) = \{x' : |x - x'|V \leq 2\}$. When the decision variables are binary, each solution $x' \subset N_2$ has exactly one or two elements (coordinates) with 0 or 1. For example, if $x = (0, 1, 1, 0, 0, 1, 0)$ and $x\prime = (0, 0, 1, 0, 1, 1, 0) \in N_1(x)$ or $x\prime = (0, 1, 1, 1, 0, 1, 0) \in N_2(x)$. Hence the modified DZZ searches a much larger neighborhood for each of its Hooke Jeeves exploration step.

VI. NUMERICAL EXPERIMENTS

A. NETWORK TOPOLOGY AND LOAD CONDITION

The topology of the radial distribution network is given in Figure 6 with $n = 13$ nodes interconnected by 12 links. This network is an expanded version of the 9-node system originally in [29], [30]. Note that prior to DER integration, a 30 MW substation is installed at node 1 with the nominal voltage $V_{DG} = 33$ kV.

We plan to expand a DG system for a period of three years (i.e. $T = 3$). The demand of 13 nodes is characterized by the mean and standard deviation, yet no assumptions are made

TABLE 1. Mean and standard deviation (Stdev) of nodal demands.

		Year 1		Year 2		Year 3	
j	Load	Mean (MW)	Stdev (MW)	Mean (MW)	Stdev (MW)	Mean (MW)	Stdev (MW)
1	D_1	0	0	0	0	0	0
2	D_2	3.435	0.515	3.538	0.531	3.644	0.547
3	D_3	3.473	0.521	3.577	0.537	3.685	0.553
4	D_4	2.063	0.309	2.125	0.319	2.189	0.328
5	D_5	1.800	0.270	1.854	0.278	1.910	0.286
6	D_6	2.310	0.347	2.379	0.357	2.451	0.368
7	D_7	2.753	0.413	2.836	0.425	2.921	0.438
8	D_8	2.535	0.38	2.611	0.392	2.689	0.403
9	D_9	2.820	0.423	2.905	0.436	2.992	0.449
10	D_{10}	2.025	0.304	2.086	0.313	2.148	0.322
11	D_{11}	2.505	0.376	2.580	0.387	2.658	0.399
12	D_{12}	2.363	0.354	2.434	0.365	2.507	0.376
13	D_{13}	1.620	0.243	1.669	0.250	1.719	0.258
sum	D	29.702	1.318	30.593	1.358	31.511	1.399

TABLE 2. Line load of year 1 and resistance and current limits of links.

l	Node pair	Mean (MW)	Stdev (MW)	R_l (Ohm)	$I_l^{\max}$ (A)
1	{1, 2}	8.97	0.795	2.43	300
2	{2, 3}	5.54	0.606	4.87	200
3	{3, 4}	2.06	0.309	3.65	100
4	{1, 5}	9.40	0.713	2.87	300
5	{5, 6}	5.06	0.539	3.04	200
6	{6, 7}	2.75	0.413	3.65	100
7	{5, 8}	2.54	0.380	3.95	100
8	{1, 9}	4.85	0.521	4.26	200
9	{9, 10}	2.03	0.304	2.78	100
10	{1, 11}	6.49	0.571	4.17	200
11	{11, 12}	2.36	0.354	4.43	100
12	{11, 13}	1.62	0.243	2.52	100

regarding the demand distribution. Table 1 lists the mean and standard deviation of the nodal demands over three years. The aggregate mean and variance of the distribution system are also obtained and listed in the last row.

The load profile of 12 links can be estimated based on the demands of its downstream nodes. Table 2 shows the mean and standard deviation of the load of twelve links in Year 1. Similar results can be obtained for Years 2 and 3. In the table, R_l is the resistance of the link between two adjacent nodes, and $I_l^{\max}$ is the maximum current that link l can accommodate. Since R_l and $I_l^{\max}$ represent the physical properties of the distribution lines, they usually do not change over the planning horizon.

B. PARAMETERS FOR WT AND PV SYSTEMS

Assume five types of DER units are available for the placement in the 13-node distribution network. These are 1.5 MW WT, 2 MW WT, 2.5 MW WT, 1 MW PV, and 1.5 MW PV. Data associated with equipment reliability, maintenance, and repair are listed in Table 3. These values are obtained based on the WT and PV reliability analysis reports in [18] and [31]. Note that η and β are the scale and shape parameters of the Weibull reliability function of DER units. The cost for a planned and a failure replacement is denoted as c_i^p and c_i^f, respectively, while t_i^p and t_i^f are the downtime duration in a planned and a failure replacement. The expected lifetime of a DER unit is assumed to be $h = 20$ years, and the loan interest rate is $r = 5\%$ compounded annually.

TABLE 3. Parameters for Weibull reliability, maintenance and downtime.

i	DER	Size (MW)	η_i (hour)	βi	c_i^p (\$) ($\times 10^3$)	c_i^f (\$) ($\times 10^3$)	t_i^p (day)	t_i^f (day)
1	WT1	1.5	10,706	1.7	6	90	3	7
2	WT2	2.0	11,264	1.8	7.5	120	3	7
3	WT3	2.5	12,560	2.0	9.5	150	3	7
5	PV1	1.0	24,000	2.1	6	70	3	6
5	PV2	1.5	20,000	1.9	10	90	3	6

TABLE 4. Cost and characteristics of WT and PV n/a=not applicable.

i	DER	a_i ($\times 10^6$)	b_i	c_i	d_i	v_c (m/s)	v_r (m/s)	v_s (m/s)
1	WT1	1.140	18	0	0	2.5	12	25
2	WT2	1.080	15	0	0	3	12	25
3	WT3	1.026	13	0	0	3	12	25
4	PV1	3.500	5	-35	0	n/a	n/a	n/a
5	PV2	3.000	5	-35	0	n/a	n/a	n/a

Table 4 summarizes the cost items associated with equipment, operation, carbon credits and subsidies for DER. In this example, only PV receives carbon credits to compensate the high installation cost, and no equipment subsidies are given to WT and PV. All cost items are node-independent, meaning $a_{ij} = a_{ik}$ for given i and $j \neq k$, so do b_{ij} and c_{ij}. The unit of a_i and d_i is \$/MW, and the unit of b_i and c_i is \$/MWh. The last three columns define the characteristic wind speeds of WT power curve. Note that v_c is the cut-in speed, v_r is the rated speed, and v_s is the cut-off speed. The values of these critical speed are based on the report from NREL [32].

In Table 5, the nodal wind speed follows the Weibull distribution, and c_w and d_w are the corresponding scale and shape parameter, respectively. Solar irradiance at each node follows the beta distribution where a_s, b_s and $s_m$are the distribution parameters. Given the wind and solar distributions, methods for computing the mean and the variance of WT and PV power output are available in [25], [33]. The substation has zero power variance because the electricity is supplied by centralized power plants. To maximize the annual energy throughput, all PV panels are oriented towards the south if in the northern hemisphere. The PV efficiency is assumed

TABLE 5. Distribution of nodal wind speed and solar irradiance.

Node	Wind Speed		Solar Irradiance		
j	c_w (m/s)	d_w	a_s	b_s	s_m (W/m^2)
1	7.82	2.73	2.93	1.92	990
2	6.66	2.64	2.96	1.63	1,053
3	7.15	2.11	3.14	1.89	979
4	6.28	2.17	2.96	1.86	986
5	6.96	1.91	2.91	1.75	1,011
6	6.80	1.97	2.90	1.72	1,013
7	7.69	1.62	3.06	1.89	1,028
8	7.31	2.23	3.05	1.79	983
9	6.20	1.81	2.93	1.92	996
10	8.01	1.78	3.06	1.89	1,028
11	6.94	2.23	3.01	1.77	990
12	6.31	1.93	2.96	1.89	1,001
13	6.96	2.03	2.98	1.94	1,015

to be $\eta_s = 0.20$, and the average operating temperature is $T_o = 45°C$. Unlike WT that operates in 8,760 hours a year, the annual operating hours for PV is 4,380 hours on average. The rated power of PV module is 120 W/m^2 under clear sky with direct sunshine.

Other parameters associated with the planning model are specified as follows: $\alpha_1 = 0.001$, $\alpha_2 = 0.9$, $\alpha_3 = 0.9$, and $\alpha_4 = 0.9$. In addition, we set $V_{\min} = 0.95\ V_{DG}$ and $V_{\max} = 1.05\ V_{DG}$, meaning nodal voltage varies within $\pm 5\%$ of its nominal value. The GEC target is $\lambda_1 = 0.1$, $\lambda_2 = 0.2$, and $\lambda_3 = 0.3$ over three years, respectively. To mimic the elimination of conventional generation, we sequentially reduce the substation capacity from 30 MW to 25 MW in $t = 2$ years, and to 20 MW in $t = 3$ years.

We solve the example problem using DZZ and NSGA-II algorithm, respectively. We choose NSGA-II as the benchmark out of two reasons. First, there are only very few methods suitable for solving discrete MOOP problems, and NSGA-II is generally available and applicable for MOOP problems with binary variables and stochastic constraints. In fact NSGA-II is often used to solve MOOP problems arising from many different fields including power engineering [34]–[36]. Second, we do not consider other MOOP methods because, as studied in [27] and [37], a zigzag search algorithm has been compared to a few other MOOP methods including pareto front approximation [38] and the normal-boundary intersection method [39]. The results in [37] show that the zigzag search is more efficient than some recently developed methods, including MO-COMPASS algorithm, standing for multi-objective convergent optimization via most-promising-area stochastic search [40]. Though there are other bio-inspired evolutionary algorithms, such as particle swarm optimization [41], they are mostly developed for continuous problems and typically slow in convergence.

The total number of design variables for the 3-year planning model is 200, including 195 binary variables and 5 continuous variables. DZZ algorithm and NSGA-II method are both implemented in Matlab computing environment. The numerical experiments are carried out on a PC workstation with 8G RAM and a 3.4GH CPU. We investigate two cases. In the first case, all nodes are assumed to be fully disconnected under catastrophic weather event. In the second case, only certain distribution lines are damaged post the extreme weather. We run four independent replications of each algorithm on the 13-node distribution network in Figure 6. The optimization results are compared and analyzed in detail below.

C. RESULTS FOR A FULLY DISCONNECTED NETWORK

In this case, it is assumed that all distribution lines are damaged post disastrous weather event. Figure 4 shows the NSGA-II optimization result for this case over a 3-year horizon of renewables integration. The Pareto front of 24 non-dominated solutions appears to be aligning along a smooth curve. The population size is 500 and the number of generation is 50 for NSGA-II.

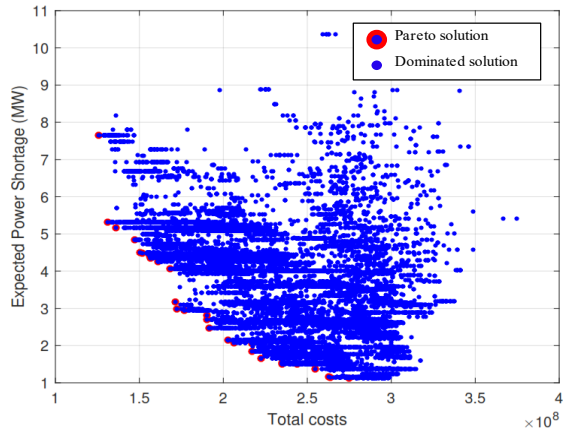

FIGURE 4. NSGA-II optimization for model P2.

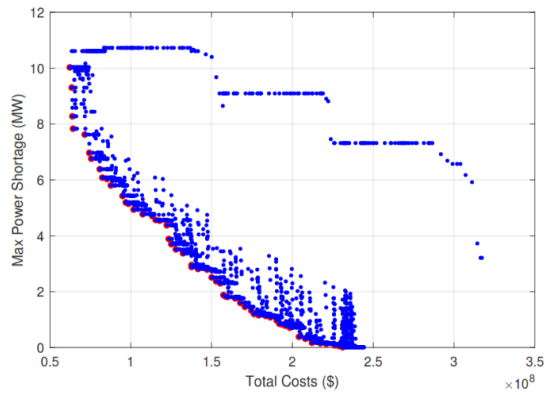

FIGURE 5. DZZ optimization for model P2.

Figure 5 depicts the optimization result of 55 Pareto solutions based on DZZ. In DZZ a local search is applied to find the first Pareto solution with the minimum cost of \$62M. Starting from this solution, DZZ applies a series of zigzag search to identify a solution path that is closely along the Pareto front. In that way DZZ can avoid evaluating many feasible solutions that are far from the Pareto front region. The optimal solutions cover a wide range of cost from \$62M to \$230M, larger than the NSGA-II frontier. Both figures show the maximum power shortage post extreme events decreases from 10 MW to zero with the increasing system investment. Table 6 summarizes the performance comparisons between DZZ and NSGA-II.

TABLE 6. Performance comparison between NSGA-II and DZZ.

	NSGA-II	DZZ
Feasible Solution evaluated	25,000	2852
Number Pareto solutions	24	55
Computation time (s)	7.12	1.08

Figure 6 shows the detailed power generation and demand at every node for a particular Pareto solution found by DZZ. Optimal sizing, siting and maintenance of WT and solar PV

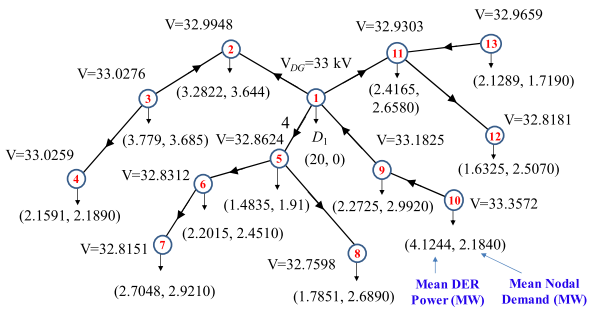

FIGURE 6. Nodal voltage and power flow for a pareto solution in Year 3.

TABLE 7. A Pareto solution obtained by DZZ.

Node	WT1	WT2	WT3	PV1	PV2
1	0	0	0	0	0
2	2	3	1	0	0
3	3	2	1	1	1
4	2	1	1	0	0
5	3	0	0	0	0
6	2	2	0	0	0
7	2	2	0	0	0
8	2	1	0	0	0
9	3	2	0	0	0
10	3	1	2	0	0
11	2	1	1	0	0
12	1	1	1	0	0
13	3	1	0	0	0
τ (hour)	5,011.5	5,066.4	5,000.3	9,975.0	6,385.0

are listed in Table 7 with the bi-objective values $(g_1, g_2) =$ (\$125M, 3.88 MW). It shows that some nodes can produce more power than their demand, and the surplus power indeed flows to their neighboring nodes, either downstream or upstream. For instance, the DER units at Node 10 generate 4.1244 MW while its demand is only 2.1840 MW. Therefore, an amount of power 1.9404 MW flows along the upstream power line (i.e. reversely) to Node 9. Node 3 is another case of which the surplus power goes to the downstream Node 4 and to the upstream Node 2. For Node 3, the power line between Nodes 2 and 4 has bidirectional power flow.

The power resilience in Figure 6 is manifested as prevention and the survivability which are reflected in the allocated DER power at each node. Take example of Table 7, the optimal allocation of WT and PV capacity to each node is listed along with the equipment maintenance interval. The nodal mean power shown in Figure 6 actually demonstrates the degree of survivability of the network. For instance, the mean power of Node 2 is 3.2882 MW. If Node 2 is isolated because its adjacent distribution lines are damaged, the local power shortage is only 3.644-3.2882=0.3558 MW.

A main advantage of the non-dominant solution set over a single objective optimization lies in the fact that the decision-maker can choose a best comprised solution by trading the cost with the network survivability. In Model P2, the capability of network survivability is manifested by the Pareto optimality front in Figure 5. If the network planner is willing to invest more budget on distributed power capacity, the maximum nodal power shortage can be further reduced.

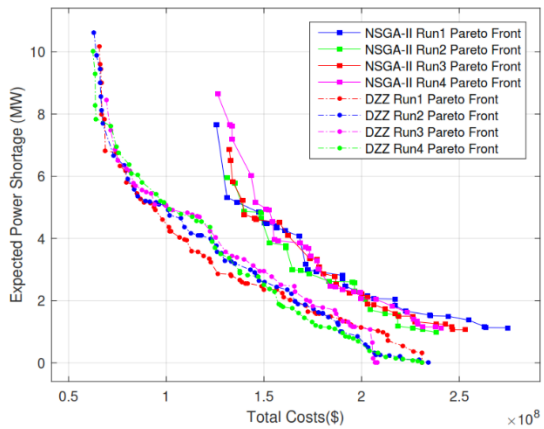

FIGURE 7. Comparison between DZZ and NSGA-II based on four runs.

Figure 7 compares the optimization performance of NSGA-II and DZZ algorithms applied for this example case with multiple replications. The plotted solutions (in the objective function space) from both algorithms are non-dominated solutions among all the evaluated solutions. For comparison purpose, we run both algorithms four times independently with different initial solutions. For all the four runs of DZZ, 2,500 to 3,000 solutions are evaluated, while NSGA-II evaluates about 25,000 solutions for each of its four runs. From the results, we see that all four DZZ runs outperform NSGA-II by locating better trade-off solutions and larger coverage of the Pareto front.

Based on our numerical experiments, the total computing times for both algorithms are approximately proportional to the number of feasible solutions evaluated. The computing time in addition to function evaluations in DZZ algorithm is negligible because it employs neighborhood search. In other words, both DZZ and NSGA-II spend the computing time mainly in evaluating the objective functions. Since a much small amount of feasible solutions are evaluated by DZZ compared to NSGA-II, the DZZ requires less amount of computational time.

D. PV COST AND CONFIDENCE LEVEL

Note that the solution listed in Table 7 indicates that PV is not favorable compared to WT. This is because the capacity cost of PV is much higher than those of WT. Suppose that PV cost is reduced to \$1.5M/MW and \$1.0M/MW, respectively, for 1 MW and 1.5 MW PV systems, optimal solutions show that more PV units will be chosen and installed. Table 8 shows a Pareto solution obtained under the reduced PV costs. There are 14 PV1 and 17 PV2 units are now installed as opposed to only 1 PV1 and 1 PV2 in Table 7.

Since the confidence levels in Equations (15)-(18) also influence the system cost and the nodal power shortage. By referring to Model P1, α_1 represents the LOLP, and the benchmark value in our numerical study is $\alpha_1 = 0.001$.

TABLE 8. A solution obtained by DZZ under reduced PV capacity cost.

Node	WT1	WT2	WT3	PV1	PV2
1	0	0	0	0	0
2	2	1	2	1	0
3	1	1	2	0	2
4	2	2	2	0	1
5	0	2	0	0	1
6	2	1	2	0	1
7	2	2	1	2	1
8	3	1	1	2	0
9	2	1	1	1	2
10	2	1	2	1	1
11	1	0	2	2	2
12	1	1	1	2	3
13	2	0	1	3	3
τ (hour)	9,049.1	9451.3	7,978.2	6,202.4	6,864.2

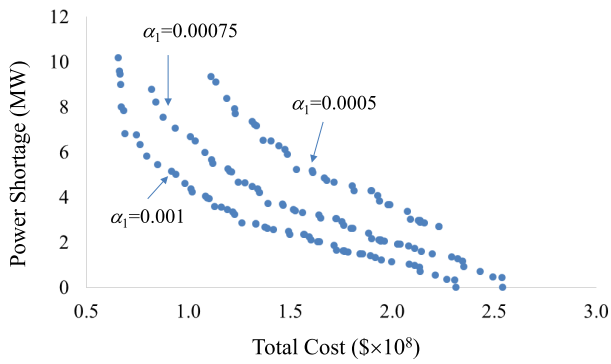

FIGURE 8. The pareto front under different value of α_1.

A smaller α_1 is always preferred as it results in a lower probability of power shortage. By looking at Equation (15), reducing α_1 requires more installation of WT and PV units locally, hence the system cost $g_1(\mathbf{x}, \tau)$ will increase. We solve Model P2 by reducing α_1 to 0.00075 and 0.0005, respectively, whereas other conditions remain unchanged. The corresponding non-dominant solution sets are presented in Figure 8 along with the Pareto front of the benchmark solution. Other confidence levels like α_2, α_3 and α_4, represent the nodal voltage, thermal stress, and renewables penetration, respectively. If one increases any of these confidence value, it is anticipated similar pareto frontiers like the case of α_1 will be obtained.

E. RESULTS OF PARTIALLY DISCONNECTED LINES

Extreme events breaking down all the distribution lines are among the worse-case scenarios, but the probability of such occurrence is very rare in reality. We consider several realistic disruptive events due to severe weather or other natural disasters that may cause some lines or components to fail. To account for varying levels of potential disruptions, for the studied 13-node network in Figure 6, we choose three representative damaging events corresponding to catastrophic, disruptive, and low disruptive scenarios respectively. More specifically, we consider three arbitrary scenarios under different levels of disruptions: $s_1 = \{(1, 2), (3, 4), (1, 5), (5, 6), (1, 9), (1, 11)\}$ has six links broken with probability $p_1 = 0.1$; $s_2 = \{(1, 2), (1, 5), (6, 7), (1, 11)\}$ has four links broken with probability $p_2 = 0.3$; and $s_3 = \{(1, 5), (1, 9)\}$ has two links broken with probability $p_3 = 0.6$. Note a nodal pair in s_k for $k = 1, 2$, and 3 represents a particular link. Overall, we want to minimize the expected total power shortage for all the network nodes. In this setting, the second objective function g_2 in Model P2 becomes:

$$g_2(\mathbf{x}, \boldsymbol{\tau}) = E_{\omega,\xi} \sum_{t=1}^{T} \sum_{s \in S} \max \left\{ \sum_{j \in s} \left[D_{jt}(\xi) - \sum_{i=1}^{m} z_{ijt} P_{ijt}(\omega) \right], 0 \right\} \times p_s. \tag{31}$$

where $S = \{s_1, s_2, s_3\}$ represents the set of three disruptive scenarios being considered, and each scenario represents a damaged network of disconnected clusters of nodes.

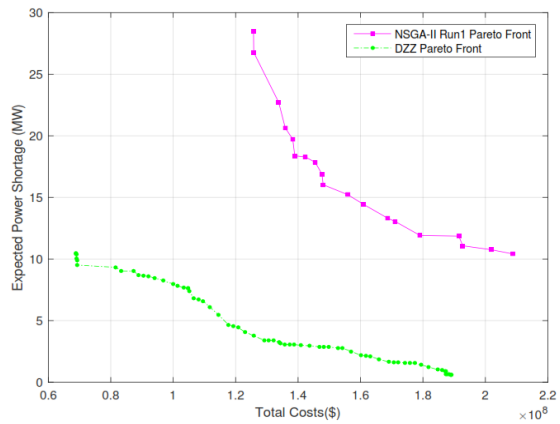

FIGURE 9. Pareto front for the three distructive scenarios.

We run Model P2 on the example problem with the consideration of three disruption scenarios. Figure 9 shows the solutions evaluated using both optimization algorithms. Note that NSGA-II needs to evaluate much more solutions (~20,000) that are all inferior to those evaluated (~2,000-3,000) in DZZ. The results for this case also indicate that DZZ outperforms NSGA-II again in terms of computational speed and solution quality.

VII. CONCLUSION

This paper proposes a multi-year, multi-criteria distributed generation expansion model to minimize the cost and maximize the power resilience against disastrous weather events. A modified direct zigzag algorithm is adopted to search for the optimal sizing, siting, and maintenance of DER units. We enhance the distribution resilience in terms of grid prevention and generation survivability in contingency. The prevention is achieved by increasing the distributed generation power, reducing the substation capacity, and implementing preventive maintenance program. The survivability is achieved by minimizing the maximum nodal power shortage across the entire distribution system. The proposed planning

model is applicable to distribution networks where lines are either fully or partially destroyed. In either case, wind- and solar-based DER units are split into island microgrid systems to power the critical loads. Since wind and solar generation does not rely on fossil fuels, this is advantageous over fuel-based generating units as the fuel lifeline is likely to be damaged in the aftermath of catastrophic events. Hence the risk of cascading failures could be largely mitigated or avoided using onsite renewable energy. The variations of load, voltage and thermal stresses are characterized by chance constraints through the central limit theorem.

Two observations are obtained from the numerical example. First, the direct zigzag search is able to explore a wider frontier and returns a set of non-dominant solutions with higher quality compared with NSGA-II. Second, the testing network indicates that 30 percent of renewable penetration can be achieved sequentially in three years by concurrently injecting WT and PV units, and reducing the substation capacity. There are several potential extensions of this work. For instance, the model can be formulated and solved in a large AC network and the results could be compared with the DC circuit. Another direction is to expand the model by incorporating fuel-based DG or batteries and analyze the tradeoff between the cost and the resilience performance in various operating scenarios.

APPENDIX

Loss of load probability (LOLP) is defined as the probability that the power supply drops below the load. We rewrite the chance constraint (15) as follows

$$\Pr\{P_t(\mathbf{x}) < D_t\} \leq \alpha_1, \quad \forall t. \tag{A1}$$

where, α_1 is the acceptable LOLP limit. Define $Y = P_t(\mathbf{x}) - D_t$, then we have

$$\Pr\{Y < 0\} \leq \alpha_1, \quad \forall t. \tag{A2}$$

and the mean and variance of Y is

$$E[Y] = E[P_t(\mathbf{x})] - E[D_t] = \mu_{P_t(\mathbf{x})} - \mu_{D_t} \tag{A3}$$

$$\sigma_Y^2 = Var(P_t(\mathbf{x})) - Var(D_t) = \sigma_{P_t(\mathbf{x})}^2 + \mu_{D_t}^2 \tag{A4}$$

According to central limit theorem, $P_t(\mathbf{x})$ and D_t follows the normal distribution, so does Y. Therefore, the deterministic counterpart of constraint (A1) or (A2) is obtained as

$$E[Y] \geq 0 + Z_{1-\alpha_1}\sigma_Y, \quad \forall t \tag{A5}$$

where $Z_{1-\alpha_1}$ is the z-score at (1-α_1)$\times$100% confidence for a standard normal distribution. By substituting Equations (A3) and (A4) into (A5), we have

$$\mu_{P_t(\mathbf{x})} \geq \mu_{D_t} + Z_{1-\alpha_1}(\sigma_{P_t(\mathbf{x})}^2 + \sigma_{D_t}^2)^{1/2}, \quad \forall t \tag{A6}$$

Similarly, under the normality condition the deterministic constraints (25) and (26) for voltage variation and thermal stress control are derived based on the corresponding chance constraints (16) and (17), respectively.

REFERENCES

[1] S. Ma, B. Chen, and Z. Wang, "Resilience enhancement strategy for distribution systems under extreme weather events," *IEEE Trans. Smart Grid*, vol. 9, no. 2, pp. 1442–1451, Mar. 2018.

[2] Y. Wang, C. Chen, J. Wang, and R. Baldick, "Research on resilience of power systems under natural Disasters—A review," *IEEE Trans. Power Syst.*, vol. 31, no. 2, pp. 1604–1613, Mar. 2016.

[3] N. L. Dehghani, Y. M. Darestani, and A. Shafieezadeh, "Optimal life-cycle resilience enhancement of aging power distribution systems: A MINLP-based preventive maintenance planning," *IEEE Access*, vol. 8, pp. 22324–22334, 2020.

[4] L. Che and M. Shahidehpour, "DC microgrids: Economic operation and enhancement of resilience by hierarchical control," *IEEE Trans. Smart Grid*, vol. 5, no. 5, pp. 2517–2526, Sep. 2014.

[5] Y. Lin and Z. Bie, "Study on the resilience of the integrated energy system," *Energy Procedia*, vol. 103, pp. 171–176, Dec. 2016.

[6] B. Ovens. (2014). *The Rise of Distributed Power*. Report of General Electric. Accessed: Nov. 10, 2017. [Online]. Available: http://www.eenews.net/assets/2014/02/25/

[7] L.-J. Yang, Y. Zhao, C. Wang, P. Gao, and J.-H. Hao, "Resilience-oriented hierarchical service restoration in distribution system considering microgrids," *IEEE Access*, vol. 7, pp. 152729–152743, 2019.

[8] Y. Xu, Y. Wang, J. He, M. Su, and P. Ni, "Resilience-oriented distribution system restoration considering mobile emergency resource dispatch in transportation system," *IEEE Access*, vol. 7, pp. 73899–73912, 2019.

[9] EPRI. *Grid Resiliency*. Accessed: Nov. 11, 2017. [Online]. Available: https://www.epri.com/#/pages/sa/grid_resiliency

[10] P. S. Georgilakis and N. D. Hatziargyriou, "Optimal distributed generation placement in power distribution networks: Models, methods, and future research," *IEEE Trans. Power Syst.*, vol. 28, no. 3, pp. 3420–3428, Aug. 2013.

[11] M. Panteli, D. N. Trakas, P. Mancarella, and N. D. Hatziargyriou, "Boosting the power grid resilience to extreme weather events using defensive islanding," *IEEE Trans. Smart Grid*, vol. 7, no. 6, pp. 2913–2922, Nov. 2016.

[12] A. Kwasinski, V. Krishnamurthy, J. Song, and R. Sharma, "Availability evaluation of micro-grids for resistant power supply during natural disasters," *IEEE Trans. Smart Grid*, vol. 3, no. 4, pp. 2007–2018, Dec. 2012.

[13] Z. Bie, Y. Lin, G. Li, and F. Li, "Battling the extreme: A study on the power system resilience," *Proc. IEEE*, vol. 105, no. 7, pp. 1253–1266, Jul. 2017.

[14] S. Ma, S. Li, Z. Wang, and F. Qiu, "Resilience-oriented design of distribution systems," *IEEE Trans. Power Syst.*, vol. 34, no. 4, pp. 2880–2891, Jul. 2019.

[15] M. Shahidehpour, X. Liu, Z. Li, and Y. Cao, "Microgrids for enhancing the power grid resilience in extreme conditions," *IEEE Trans. Smart Grid*, vol. 8, no. 2, pp. 589–597, Jun. 2016.

[16] K. Fischer, F. Besnard, and L. Bertling, "Reliability-centered maintenance for wind turbines based on statistical analysis and practical experience," *IEEE Trans. Energy Convers.*, vol. 27, no. 1, pp. 184–195, Mar. 2012.

[17] T. Jin, Y. Tian, C. W. Zhang, and D. W. Coit, "Multicriteria planning for distributed wind generation under strategic maintenance," *IEEE Trans. Power Del.*, vol. 28, no. 1, pp. 357–367, Jan. 2013.

[18] H. Guo, S. Watson, P. Tavner, and J. Xiang, "Reliability analysis for wind turbines with incomplete failure data collected from after the date of initial installation," *Rel. Eng. Syst. Saf.*, vol. 94, no. 6, pp. 1057–1063, Jun. 2009.

[19] E. Collins, M. Dvorack, J. Mahn, M. Mundt, and M. Quintana, "Reliability and availability analysis of a fielded photovoltaic system," in *Proc. 34th IEEE Photovoltaic Spec. Conf. (PVSC)*, Jun. 2009, pp. 1–6.

[20] NREL. (2016). *Distributed Generation Renewable Energy Estimate of Costs*. National Renewable Energy Laboratory Report. Accessed: Jun. 11, 2018. [Online]. Available: https://www.nrel.gov/analysis/tech-lcoe-re-cost-est.html

[21] T. J. Overbye, X. Cheng, and Y. Sun, "A comparison of the AC and DC power flow models for LMP calculations," in *Proc. 37th Annu. Hawaii Int. Conf. Syst. Sci.*, Jan. 2004, pp. 1–9. Accessed: Jun. 1, 2018. Online]. Available: http://citeseerx.ist.psu.edu/viewdoc/download?doi=10.1.1.102.8273&rep=rep1&type=pdf

[22] B. Stott, J. Jardim, and O. Alsac, "DC power flow revisited," *IEEE Trans. Power Syst.*, vol. 24, no. 3, pp. 1290–1300, Aug. 2009.

[23] T. Jin, Y. Yu, and E. Elsayed, "Reliability and quality control for distributed wind/solar energy integration: A multi-criteria approach," *IIE Trans.*, vol. 47, no. 10, pp. 1122–1138, Oct. 2015.

[24] U. S. Department of Commerce (US DoC). (2013). *Economic impact of Hurricane Sandy* prepared by Economics and Statistics Administration Office of the Chief Economist. Accessed: Dec. 25, 2016. [Online]. Available: http://www.esa.gov/sites/default/files/sandyfinal101713.pdf

[25] Z. Liu, F. Wen, and G. Ledwich, "Optimal siting and sizing of distributed generators in distribution systems considering uncertainties," *IEEE Trans. Power Del.*, vol. 26, no. 4, pp. 2541–2551, Oct. 2011.

[26] V. Hengsritawat, T. Tayjasanant, and N. Nimpitiwan, "Optimal sizing of photovoltaic distributed generators in a distribution system with consideration of solar radiation and harmonic distortion," *Int. J. Electr. Power Energy Syst.*, vol. 39, no. 1, pp. 36–47, Jul. 2012.

[27] H. Wang, "Direct zigzag search for discrete multi-objective optimization," *Comput. Oper. Res.*, vol. 61, pp. 100–109, Sep. 2015.

[28] K. Deb, A. Pratap, S. Agarwal, and T. Meyarivan, "A fast and elitist multiobjective genetic algorithm: NSGA-II," *IEEE Trans. Evol. Comput.*, vol. 6, no. 2, pp. 182–197, Apr. 2002.

[29] M.-R. Haghifam, H. Falaghi, and O. P. Malik, "Risk-based distributed generation placement," *IET Gener., Transmiss. Distrib.*, vol. 2, no. 2, p. 252, Mar. 2008.

[30] W. El-Khattam, K. Bhattacharya, Y. Hegazy, and M. M. A. Salama, "Optimal investment planning for distributed generation in a competitive electricity market," *IEEE Trans. Power Syst.*, vol. 19, no. 3, pp. 1674–1684, Aug. 2004.

[31] Z. Tian, T. Jin, B. Wu, and F. Ding, "Condition based maintenance optimization for wind power generation systems under continuous monitoring," *Renew. Energy*, vol. 36, no. 5, pp. 1502–1509, May 2011.

[32] T. Stehly, P. Beiter, D. Heimiller, G. Scott. (2018). *The 2017 Cost of Wind Energy Review*. National Renewable Energy Laboratory Report. Accessed: Sep. 21, 2019. [Online]. Available: https://www.nrel.gov/docs/fy18osti/72167.pdf

[33] Z. M. Salameh, B. S. Borowy, and A. R. A. Amin, "Photovoltaic module-site matching based on the capacity factors," *IEEE Trans. Energy Convers.*, vol. 10, no. 2, pp. 326–332, Jun. 1995.

[34] M. Karimi and M. R. Haghifam, "Risk based multi-objective dynamic expansion planning of sub-transmission network in order to have eco-reliability, environmental friendly network with higher power quality," *IET Gener., Transmiss. Distrib.*, vol. 11, no. 1, pp. 261–271, Jan. 2017.

[35] H. Bilil, G. Aniba, and H. Gharavi, "Dynamic appliances scheduling in collaborative MicroGrids system," *IEEE Trans. Power Syst.*, vol. 32, no. 3, pp. 2276–2287, May 2017.

[36] S. M. Mazhari, H. Monsef, and R. Romero, "A multi-objective distribution system expansion planning incorporating customer choices on reliability," *IEEE Trans. Power Syst.*, vol. 31, no. 2, pp. 1330–1340, Mar. 2016.

[37] H. Wang, "Zigzag search for continuous multiobjective optimization," *INFORMS J. Comput.*, vol. 25, no. 4, pp. 654–665, Nov. 2013.

[38] J.-H. Ryu, S. Kim, and H. Wan, "Pareto front approximation with adaptive weighted sum method in multiobjective simulation optimization," in *Proc. Winter Simulation Conf. (WSC)*, Dec. 2009, pp. 623–633.

[39] I. Das and J. E. Dennis, "Normal-boundary intersection: A new method for generating the Pareto surface in nonlinear multicriteria optimization problems," *SIAM J. Optim.*, vol. 8, no. 3, pp. 631–657, Aug. 1998.

[40] H. Li, L. H. Lee, E. P. Chew, P. Lendermann, P., "Mo-compass: A fast convergent search algorithm for multi-objective discrete optimization via simulation," *IIE Trans.*, vol. 4, no. 11, pp. 1153–1169, 2015.

[41] M. R. Sierra and A. A. C. Coello, "Improving PSO-based multi-objective optimization using crowding, mutation and ?-dominance," *Evolutionary Multi-Criterion Optimization*. Berlin, Germany: Springer, 2005, pp. 505–519.

HONGGANG WANG received the B.Sc. degree in power engineering from Shanghai Jiao Tong University, Shanghai, China, in 1996, the M.Sc. degree in manufacturing engineering from the University of Missouri–Rolla, in 2004, and the Ph.D. degree in operations research from Purdue University, West Lafayette, IN, USA, in 2009. He worked as a Postdoctoral Scholar in energy resources engineering with Stanford University, for two years. He is currently an Assistant Professor of technology and operations management with California State Polytechnic University-Pomona. He received the IBM Faculty Award 2012 and the Faculty Award from Tracy Energy, in 2016, for his work in energy systems research. He also received the 2016 Best Paper Award at Geothermal Research Council annual meeting, Sacramento, CA, USA.

TONGDAN JIN (Senior Member, IEEE) received the B.S. degree in automation engineering from the Shaanxi University of Science and Technology, Xi'an, China, and the M.S. degree in electrical and computer engineering and the Ph.D. degree in systems engineering from Rutgers University. He is currently an Associate Professor with the Ingram School of Engineering, Texas State University. He is the author of the new book *Reliability Engineering and Services* (Wiley, 2019). His research interests and publications are in areas of renewable energy, sustainable supply chain, and reliability optimization. He was a recipient of best paper awards in several international conferences, including the Evans-McElroy Best Paper in the 2014 Annual Reliability and Maintainability Symposium. His research projects are funded by NSF, USDA, the U.S. Department of Education, and private foundations. He is a member of INFORMS and IISE.